Available online at www.sciencedirect.com
ScienceDirect
International Journal of Heat and Mass Transfer 51 (2008) 3442–3459
International Journal of HEAT and MASS TRANSFER
www.elsevier.com/locate/ijhmt

Instantaneous and objective flow regime identification method for the vertical upward and downward co-current two-phase flow

Jae Young Lee [a], Mamoru Ishii [b,*], Nam Seok Kim [a]

[a] School of Mechanical and Control Engineering, Han Dong University, Pohang, Republic of Korea
[b] School of Nuclear Engineering, Purdue University, West Lafayette, USA

Received 20 October 2005
Available online 15 February 2008

Abstract

An instantaneous and objective flow regime identification method for the two-phase flow is represented in the paper. The previous methods have been evolved to be an objective by replacing the heuristic determination using the sensor signals in terms of the statistical indexes. However, the flow pattern in the rapid transient or the inherently unstable flow such as the flow in the microgravity cannot be identified because of the observation time for the statistical meaning. The design of the neural network fed by the preprocessed impedance signals of the cross-sectional void fraction is proposed here to satisfy the requirement of both objective and an instantaneous identification. For the preprocessing, the both feed forward neural network and the self-organized neural network as an objective reasoning engine were tested using the experimental data for both upward and downward two-phase flow in the pipes with the inner diameter of 25.4 mm and 50.8 mm. It was found that the proposed flow regime identifier could successfully identify the flow regime using the short term observation data within 1 s. Furthermore, the obtained flow regimes were in a good agreement with the Mishima–Ishii criteria for the upward two-phase flow. However, for the downward flow, it was found that the current flow regimes are in reasonable agreement with the Usui criteria for the slug flow region, only. Other flow regimes have strong dependency on the pipe diameter and some phenomena related to the kinematic wave propagation which was not considered reasonably in the previous criteria. Therefore, theoretical studies to build up the transition criteria for the co-current downward two-phase flow are recommended.

Keywords: Two-phase flow; Flow regime; Objective; Instantaneous; Neural network; Probability distribution function

1. Introduction

The flow pattern of the two-phase flow varies according to the mass flow rate of each phase. Most of interactions among phases and solid boundary are strongly dependent upon the flow pattern. For the design and an analysis of the system in two-phase flow, it is essential to gear up the knowledge of the flow pattern. In the nuclear industry, the two-fluid formulation [1] has widely been used as the best estimate method in the safety analysis. However, the two-fluid model is furnished by many interfacial transfer terms which are highly sensitive to the flow pattern. In each step of calculation, the computer codes of the two-fluid model evaluate the flow regime with the calculated parameters and determine the transfer rates of parameters for the next time step. The code may have uncertainties and spurious transient due to the flow regime map used. Therefore, the study of the flow regime identification and transport equation of interfacial area concentration has been studied intensively. With the clue of the recent progress in the transport formulation of the interfacial area concentration to go upon removing the flow regime map in the two-fluid code has been investigated intensively [2].

However, the flow regime map in the two-fluid code needs studies to make it more objective and applicable to the rapid transient. As for the objectiveness, the progress

* Corresponding author. Tel.: +1 765 494 4587.
E-mail address: ishii@ecn.purdue.edu (M. Ishii).

0017-9310/$ - see front matter © 2008 Published by Elsevier Ltd.
doi:10.1016/j.ijheatmasstransfer.2007.10.037

Nomenclature

$d_i = \|x - W_i\|^2$	Euclidean distance
J_g	superficial gas velocity
J_f	superficial liquid velocity
$L_{pattern}$	characteristic length of two-phase flow
O_h	the output value of the hth hidden node
$u_{pattern}$	characteristic velocity of the faster phase
W_h	connection weights between nodes of hidden and output layer
W_{ij}	ijth weight
$W_i^T = (W_{i1}, W_{i2}, \ldots, W_{iN})^T$	ith weight vector
W_{nh}	connection weights between nodes of hidden and input layer
W_o, W_{oh}	threshold or bias
x	input vector
y	output vector
$\hat{y}$	reference output vector

Greek symbols

δ_i	delta function (unity for the winning neuron i) but is zero otherwise
η ($\eta > 0$)	learning rate
θ	adjusting parameter
$\sigma(x)$	sigmoid function $\sigma(x) = \frac{1}{1+e^{-x/\theta}}$
τ_{patt}	pattern characteristic time
τ_{system}	system transient time

has been made to drift out the visual observation [3–6] to the use of the sensor signals [7], and the heuristic determination of the flow regime based on the probability density function (PDEF)[1] has been widely used [8]. To make the flow regime identification more objective, recent progress in the cognition science has been employed. Mi et al. [9] identified flow regimes using neural network with the characteristics of the PDEF such as the mean, variance, and skewness. However, it took longer than 60 s for the data sampling to satisfy the statistical requirement. Considering the recent studies on the two-phase flow in the microgravity in line with the program for the space propulsion using nuclear power, and the safety analysis of some rapid transients in the hypothetic incident of the nuclear power plant, it is rather longer time span for the flow pattern identification. Therefore, the present study was made to develop a method to identify the flow regime in an instantaneous manner with the short period of observation within one or one second and in an objective manner using the neural network. Many issues that rose in the present method will be discussed here such as the preprocessing of the input data, the optimization of the neural network structure, the supervising and self-organization, and the flow regime identification. It may be expected that the present method could be a useful tool for evaluation of the model of the interfacial area concentration for the short time variation as well.

2. Method of instantaneous and objective flow regime identification

The objective and instantaneous flow regime identification are simply made by inputting the signals of short period of observation which is recognized for the observer as the instantaneous comparing to the characteristic time of the phenomena to the neural network to avoid heuristic determination. Therefore, the issues to be discussed are the meaning of the instantaneous observation, the preprocessing of input signals, the sort of neural network, the optimization and sensitivity of the structure of the neural network.

2.1. An instantaneous observation and the preprocessing of the input signals

For the instantaneous flow regime identification, the observation time needs to be defined. Fig. 1 illustrates the typical air–water flow regimes observed in vertical 25.4 mm diameter pipe. The flow regimes in the first, second, third, fourth, and fifth figures from the left are bubbly, cap bubbly, slug, churn turbulent, and annular flows, respectively. As the characteristic length scale, the size of specific bubbles such as discrete bubble, cap bubble, and Taylor bubble can be selected in the bubbly, cap bubbly, and slug flow pattern.

The relatively much shorter observation time than the time to produce the probability density function (PDEF) satisfying the statistical requirement, may be the acceptable meaning for the instantaneous identification. But the time should be longer enough to represent the specific characteristics of the flow regime. For instance, if we observe the slug flow as shown in Fig. 2, the shorter time than the characteristic time would lead for the flow regime identifier to tell the other flow pattern such as annular flow or the bubbly flow. The characteristic time for the slug flow should be longer than the observation time at least one large Taylor bubble and the slug with discrete bubbles. Therefore, the time can be determined by dividing the total length of the characteristic pattern by the fast representative velocity, in this case, the Taylor bubble velocity. Once we knew the characteristic length of the two-phase flow, $L_{pattern}$, and the characteristic velocity of the faster phase, the minimum time for the flow regime identifier would be

$$\tau_{patt} = \frac{L_{pattern}}{u_{pattern}}. \quad (1)$$

[1] It is normally abbreviated as PdF but in the present paper we use PDEF to distinguish the probability distribution function as PDSF.

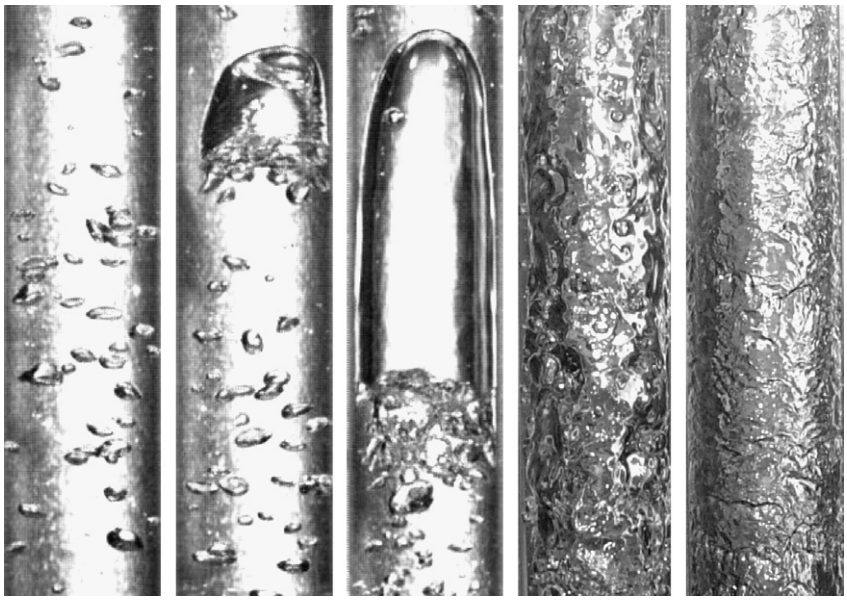

Fig. 1. Typical air–water flow images observed in a vertical upward two-phase flow in a pipe of 25.4 mm diameter.

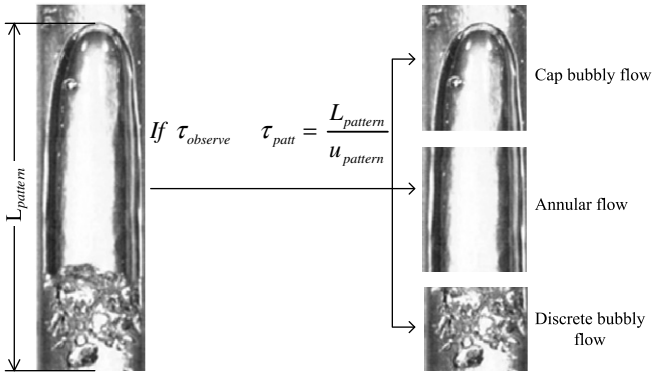

Fig. 2. The effect of the observation time τ_{obs} on the flow regime identification: the observation time should be longer than the flow pattern characteristic time τ_{patt}.

However, τ_{patt} is defined in the sense of the quasi-steady state. The two-phase flow under the rapid transient may be shorter than τ_{patt}. For instance, the downward two-phase flow in a relatively large pipe has the flow regime of unstable in which small variation of the gas flow rate induces sudden flow pattern change from annular flow to the bubbly flow. The front shock wave transport along the pipe and two different flow patterns coexist with the boundary of the shock wave. Except such a rapid transient, the system dynamics take longer response time than the above flow pattern specific time. It is reasonable that the time for the instantaneous flow regime identifier should be longer than the minimum of the pattern characteristic time, τ_{patt} and system transient time, τ_{system}:

$$\tau \geqslant \min(\tau_{patt}, \tau_{system}). \quad (2)$$

In the present study, only the steady state data were used in the flow regime study. The flow regime in the system transient is out of the scope. The minimum characteristic time was less than 1 s in the present study, which is short enough to be called an instantaneous when we compare it with the previous observation time of 60 s for the PDEF identification.

The second important concept to be employed in the present study is the preprocessing of the data. Since the present method is designed to directly input the data into the neural network, so to make the problem feasible in the engineering sense, we need to consider the limitation and the way not to make the neural network be confused by the small variation of signals. For these reasons, two steps of preprocessing are taken: the data down sampling and data sorting. Down sampling was made to reduce the number of input nodes which is needed to make better convergence of the neural network because of the few output nodes representing the specific flow regimes. Sorting the data according to the magnitude of the signals will enhance the learning of the neural network to make the clear flow pattern identification. Without sorting the data, the sampling data has random initial and final values according to the initial and final time of the sampling time. The different boundary condition in the time sequential data could be a cause of the confusion to the neural network.

2.1.1. Down sampling

Even though we perform short period of measurement, fast sampling produces large number of data. To input the large number of data, however, the neural network needs the large number of input nodes, which will be the cause of heavy computational burden and poor convergence characteristics. Therefore, it is necessary to reduce the number of data without losing the physical characteristics. This data reduction will improve the structure of the neural network by reducing the number of input nodes,

which is useful in fast convergence as well as low computational burden in iteration. Many methods have been developed for data reduction in the signal processing field, however, in the present study, we simply employ classical filter based on the Nyquist sampling theorem. If we furnish more advanced method than the Nyquist sampling theorem, it will be an improvement of the present method.

The Nyquist sampling theorem proclaimed when the data are selected from the raw data with the two times faster sampling frequency than the maximum frequency of the original analog signals, the original signals could be recovered without distortion. The maximum frequency of the raw data is determined using the fast Fourier transformation. For instant, the maximum frequency for the slug flow and churn flow in this study was around 50 Hz in the present experimental data. Thus, Nyquist criteria ask the sampling frequency of 100 Hz. It was found that after data reduction, the characteristics of the slug flow such as the existence of bubbles and large slug peak were well preserved as expected.

2.1.2. Data sort for the probability distribution function

As aforementioned, the characteristics of signals from sensor, rather than the visual observation, make the flow regime identification more objective. However, the time for the observation should be longer than the time to ensure the statistical reliability. If we have the time scale for the statistical meaning, τ_{stat}, we need to observe the flow longer than this time period. There is no guarantee that this time is shorter than the transient time, τ_{phe}.

At this moment, it is noteworthy that the neural networks have merits of objectivity as much important as the robustness in decision. In other word, the neural network can make decision with imperfect data in the standard of statistical rigor. If the neural network is adopted for the flow pattern identification, there is no reason not to use this character of relaxed requirement on input data, i.e. the data observed in a shorter time than the statistical time scale. Therefore, in this work, we tried to directly input the signals to the neural network rather than the selected parameters of probability density function [10]. Total information including noise recognized by the neural network will produce the proper classification even under the instantaneous time scale, Eq. (1), and shorter than the statistical time scale.

If the signals are directly input to the neural network, its initial and final data are given in an arbitrary manner depending on the observation starting time. This arbitrariness could be a source of confusion to the neural network. This needs the preprocessing of the raw signals. If we employ the probability density function (PdF, or PDEF) and input it directly to the neural network, then at least the floating problem of initial and final values can be solved. However, there are possible spurious peaks due to imperfect data and noise when we use the small number of data. In the present work, we used the probability distribution function (PDSF) rather than PDEF, which is prepared by sorting the data according to their magnitude. Fig. 3 illustrates the difference of the PDEF and PDSF and the method to produce the PDSF. As an example, a slug flow (Fig. 3a) is monitored by the impedance meter. The time sequential signals are depicted in Fig. 3b. The probability density function based on the magnitude of the impedance is obtained by measure the probability to find the signal in a certain magnitude of impedance as shown in Fig. 3c. The probability density function of the void fraction signals has been widely used due to it has different shape for different flow regime. Furthermore, the initial value and final value are not changed by the measurement situation. However, Fig. 3d is constructed

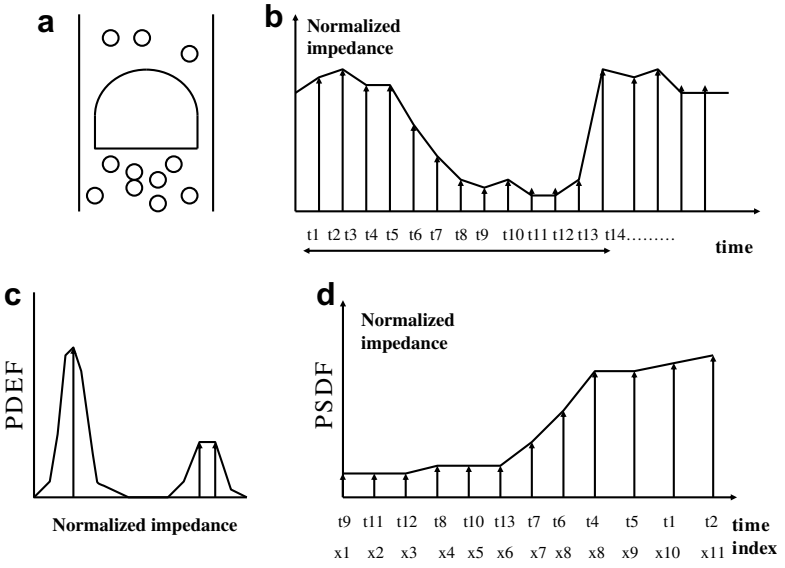

Fig. 3. Construction of PDEF and PDSF from the time sequential impedance signals for void fraction. (a) Bubble distribution; (b) time sequential data of impedance signals; (c) probability density function of impedance signals; (d) the sorted data according to magnitude (probability distribution function).

just by sorting data with its magnitude so that index in the figure means just the sequence of the sorted data. It is correspondent with the probability distribution function to find the certain magnitude of signals. This simple method of construction provides us three benefits:

– Insensitive to the statistical requirement compare to PdF, so we can reduce the observation time.
– Due to its monotonic variation as shown in Figs. 4c–8c, down sampling of the data can be easily made to reduce the number of input nodes of neural network for the fast estimation.
– The shape of the PDSF is less sensitive than the original time sequential data so that neural network is hard to be confused.

The comparisons among the impedance signals, the probability distribution function and the probability density function for the typical bubbly, cap bubbly, slug, churn, and annular flows are depicted in Figs. 4–8. As expected, both functions represent the character of the specific flow regime. The one sharp peak at high impedance value are shown in PDEF (Fig. 4b) for the bubbly flow which makes high and smooth plateau in PDSF as shown in Fig. 4c in which index means sorted time sequence according to the magnitude of the impedance. The cap bubbly flow has two peaks in PDEF as shown in Fig. 5. However, the PDSF shows a jump in the middle. The slug flow also has two peaks in PDEF as shown in Fig. 6; the left peak of slug flow is higher than the peak of cap bubbly flow. Then the PDSF shows a jump in the middle, more

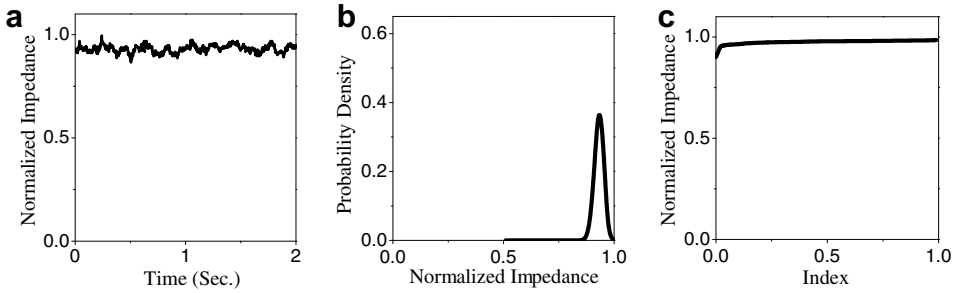

Fig. 4. The signal characteristics for the bubbly flow. (a) The void-impedance signal; (b) the probability density function for 60 s data observation; (c) the probability distribution function for 1 s data observation.

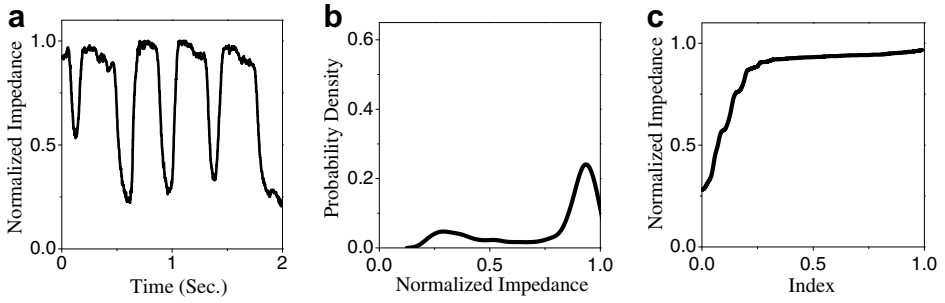

Fig. 5. The signal characteristics for the cap bubbly flow. (a) The void-impedance signal; (b) the probability density function for 60 s data observation; (c) the probability distribution function for 1 s data observation.

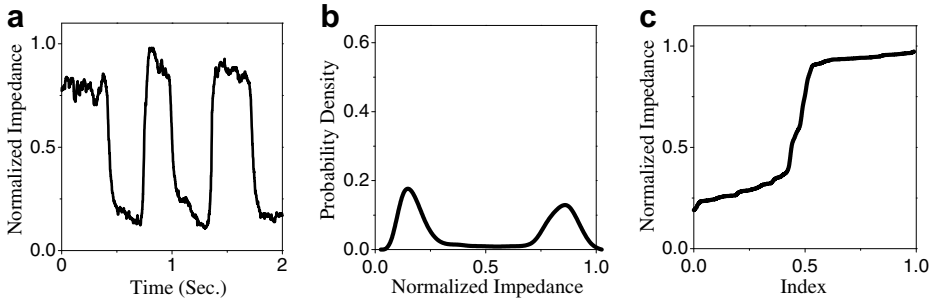

Fig. 6. The signal characteristics for the slug flow. (a) The void-impedance signal; (b) the probability density function for 60 s data observation; (c) the probability distribution function for 1 s data observation.

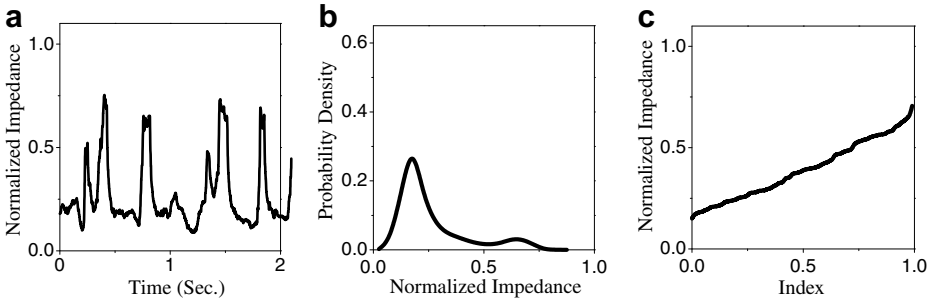

Fig. 7. The signal characteristics for the churn flow. (a) The void-impedance signal; (b) the probability density function for 60 s data observation; (c) the probability distribution function for 1 s data observation.

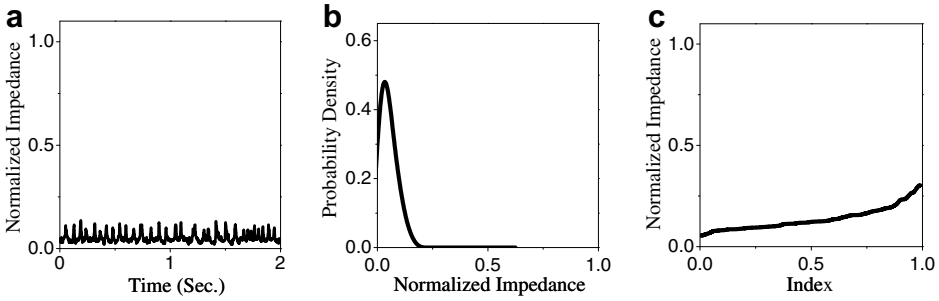

Fig. 8. The signal characteristics for the annular flow. (a) The void-impedance signal; (b) the probability density function for 60 s data observation; (c) the probability distribution function for 1 s data observation.

sharply. Therefore, the neural network can identify the difference among the bubbly flow, cap bubbly flow and slug flow. Fig. 7 shows the probability functions for the churn flow. There are multi-peaks in PDEF but PDSF shows a monotonic increase of the impedance value. Annular flow shows the similar trends to the bubbly flow except the corresponding impedance value which is lower than bubbly flow to represent the high void fraction as shown in Fig. 8.

From this discussion, it can be said that the present probability distribution function which has not been widely used for the flow pattern analysis is capable of being useful for this purpose, and furthermore, it is more stable to the imperfection of data due to the small number of data and noise. This probability distribution function and neural network make a good compatibility to achieve the purposes of the objective and instantaneous flow pattern identification.

2.2. Objectivity and neural network

The objectivity of the flow regime identification has been greatly increased by employing the neural network which provides objective decision to the previous heuristic decision based on the PDEF shape. Mi et al. [9] used three characteristics of PDEF as the input to the neural network and reported the successful identified the flow regime map. In the present study, we also use the neural networks but the number of input nodes is larger than Mi et al.'s work due to the direct input of the preprocessed data. In the present section, brief introduction of the supervised neural network and unsupervised neural network used here is made. For the present specific purpose, some noteworthy experiences in the optimization of the neural network will be explained.

2.2.1. Supervised neural network and optimization

The supervised neural network is the feed forward multi-layered neural network with one hidden layer. In the general neural network, it needs at least input layer and output layer. There are many types of neural network according to the method to connect input and output layers. One can insert many hidden layers in between the input layer and output layer like brain in our body which collects input and processes them and orders organ to react based on the decision. In case of feed forward neural network, since the network without hidden layer is supposed to be just a general linear model, the network with one hidden layer is most widely used due to its relative simple structure and it is close to projection pursuit regression in the statistical analysis. The non-linearity and relaxed statistical requirement of the data for this neural network provides a good performance in the cognition activity.

The schematic diagram to show the structure of the present feed forward neural network is shown in Fig. 9; the sorted data are input to the input layer to excite the output nodes. The nodes of the largest excitement determine the flow pattern corresponding to the node. However, when the data is in the transition border, it often produces

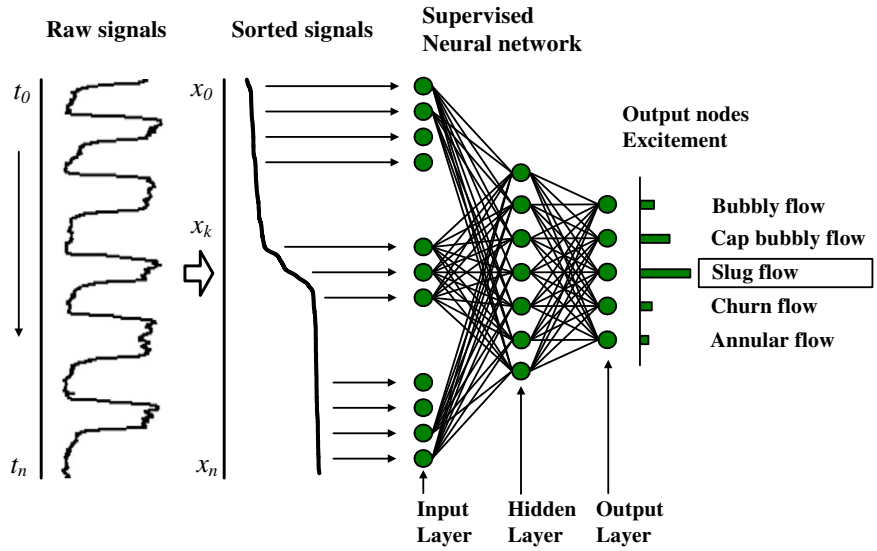

Fig. 9. The schematic diagram of the supervised neural network for the instantaneous and objective flow regime identification.

multiple excitements of the several output nodes. In this case, the data can be counted as the unidentified or transition. This can be a different character of the supervised method comparing to the unsupervised network in which the neural network produce only one winner node even at the border of competitive flow regimes.

The direct input of this data needs a large number of input nodes, which were tried from several thousands to several hundred, and output nodes are fixed to five. The determination of the excitement of neurons follows the standard method. The determination of the number of hidden nodes in the hidden layer is imperative to make good convergence and proper pattern identification. In the present study, we tried to find the number of hidden nodes showing a good convergence.

To illustrate this, let us consider a three-layer feed forward neural network with N input nodes, H hidden nodes, and one output node as shown in Fig. 10. The output from this neural network is determined by a logistic sigmoid function:

$$y = \sigma\left(\sum_{h=1}^{H} O_h \cdot W_h + W_o\right), \tag{3}$$

where the hyperbolic tangent sigmoid function $\sigma(x)$ is defined with the shape adjusting parameter θ:

$$\sigma(x) = \frac{1}{1 + \mathrm{e}^{-x/\theta}}. \tag{4}$$

O_h is the output value of the hth hidden node which is determined by the activation of the input nodes as a sigmoid function:

$$O_h = \sigma\left(\sum_{n=1}^{N} x_n \cdot W_{n,h} + W_{oh}\right). \tag{5}$$

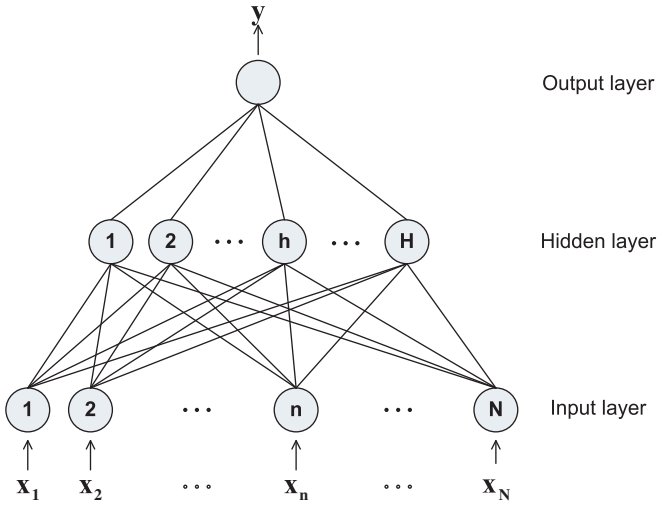

Fig. 10. Structure of typical feed forward back-propagation neural network with one hidden layer and one output node.

W_h are the connection weights between nodes of hidden and output layer, and W_{nh} are the connection weights between nodes of hidden and input layer. Also, W_o and W_{oh} serves as a threshold or bias.

During cycles of training, the weights of networks are updated in such a way that the error, $\sum(y - \hat{y})^2$, the difference between the desired response $\hat{y}$ and the computed response y, is minimized to required threshold.

Training is performed using the back-propagation algorithm. That is the input used as activation for the input layer and it is propagated to the output layer. The received output is then compared to the desired output and an error value is calculated for each node in the output layer. The weights on edges going into the output layer are adjusted by a small amount relative to the error value. This error is propagated backwards through the network to correct edge weights at all levels. Through iteration, the error

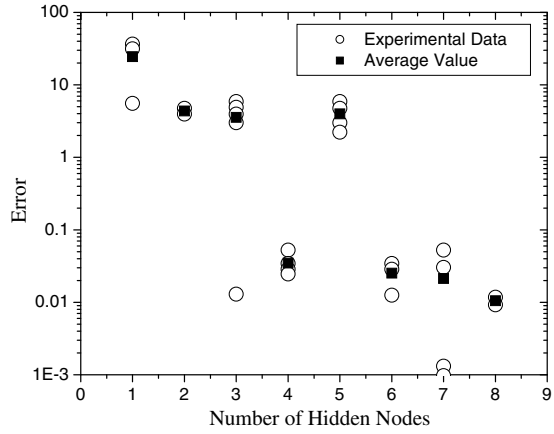

Fig. 11. The sensitivity study for the hidden layer optimization.

decreases and the training of the neural network results in a certain level of error. In the present study, we can optimize the neural network by finding the number of hidden nodes which give us small error and fast response. Fig. 11 illustrates the converged error in the back-propagation training the neural network. It is interesting that the number of hidden nodes for low error and good performance considering the calculation time was four and seven. However, the most stable prediction was made by seven hidden nodes in our experience as noted in Lee et al. [11].

2.2.2. Unsupervised neural network and optimization

Kohonen's self-organized neural network (KSOM) has been used for clustering, visualization, and abstraction [12]. The basic concept behind the KSOM is the preservation of topology, in other word the relation among data. A KSOM is an one active layer neural network consisting of a multidimensional array of neurons (usually two-dimensional). Each neuron in the grid is also an output neuron. The neurons are connected only with their closed neighbors in the array according to a prescribed topological scheme. The KSOM is trained through unsupervised competitive learning using a 'winner takes it all' policy. Due to the limited number of output nodes requested for the flow regime map, one-dimensional Kohonen self-organized neural network, one-dimensional output layer is suited. As shown in Fig. 12, a one-dimensional KSOM has two layers with input $x = (x_1, x_2, \ldots, x_N)$ and output $y = (y_1, y_2, \ldots, y_O)$. For the ith output neuron, y_i is determined by

$$y = \sum_{j=1}^{N} W_{ij} x_j = W_i^{\mathrm{T}} x, \tag{6}$$

where W_{ij} is the ijth weight and $W_i^{\mathrm{T}} = (W_{i1}, W_{i2}, \ldots, W_{iN})^{\mathrm{T}}$ is the ith weight vector. To train KSOM, the wining output neuron is determined first by comparing the similarity between the input x and the weight vector $\{W_i^{\mathrm{T}}, i = 1, \ldots, O\}$. The wight vector of the winning output neuron is then updated. As a measure of similarity between two vectors, the Euclidean distance (Kohonen [12]) is commonly used:

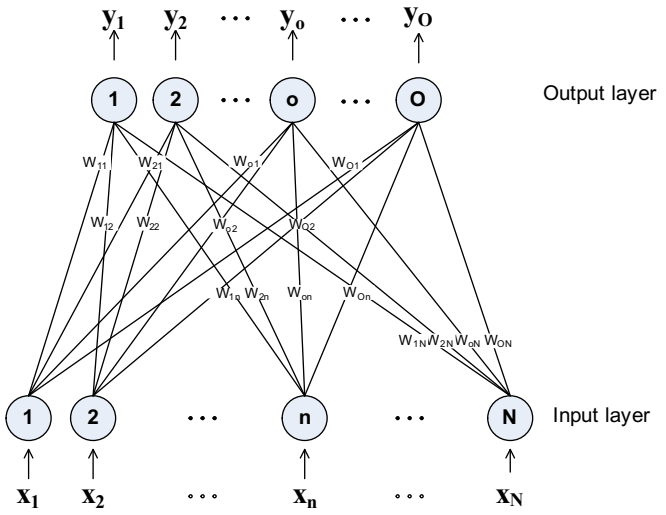

Fig. 12. One-dimensional topology of Kohonen self-organizing map.

$$d_i = \|x - W_i\|^2. \tag{7}$$

The output neuron with the minimum distance become winner and the weight vector of the winner neuron are updated as follows:

$$W_{i,\mathrm{new}} = W_{i,\mathrm{old}} + \eta(x - W_{i,\mathrm{old}})\delta_i, \quad i = 1, \ldots, O, \tag{8}$$

where η ($\eta > 0$), is the learning rate, and δ_i is unity for the winning neuron that has the smallest d_i, but is zero otherwise. The iteration is made until the variation of the weight vector approaches below a certain threshold.

The network structure is represented in Fig. 13. The output nodes are not correspondent to the flow regimes directly; rather they just represent the similar clusters of the data. In other word, the present KSOM has no explicit information on the flow regime from the result. Therefore, after getting clusters, post works are needed to resolve the character of the cluster, in this case, the corresponding flow regime. These can be made by the heuristic determination by observing the raw signals or the comparison with the results of supervised neural network.

Therefore, the result strongly depends on the number of clusters, i.e. the number of output nodes. This number cannot be determined by the learning efficiency like the supervised neural network, because it depends on the flow character, diameter of pipe, etc. As discussed in the results section, the correspondence of the clusters and flow regimes do not show the similar trends as the pipe diameter changes.

3. Experimental facility for upward and downward two-phase flow

3.1. Flow loop

The two-phase flow experiment was performed by using a flow loop installed at Thermal-hydraulics and Reactor Safety Laboratory in Purdue University. The experimental

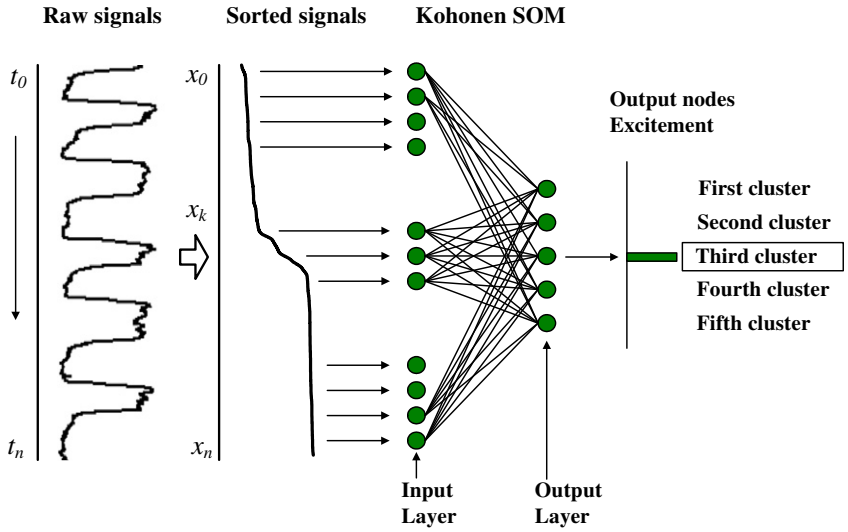

Fig. 13. Structure and clustering concept of the Kohonen's self-organized neural network for the instantaneous and objective flow regime identification.

loop presented in this investigation is an adiabatic, a vertical, air–water system. The schematic diagram of the experimental loop is shown in Fig. 14. The experimental loop consists of the two test sections, which are 2.54 cm ID and 5.08 cm ID round acrylic tubes whose total lengths are $L/D = 150$ and 75, respectively. Transparent acrylic is employed for the entire test section so that the flow can be observed at any location.

An air–water mixture injection unit is used at the top and the bottom of each test section so that the loop is capable of operating both upward and downward flow experiments. This is one of the most unique features of this experimental loop.

Water flow is supplied by a 18.65 KW centrifugal pump manufactured by Goulds Pump, which is capable of delivering up to 1514 l of liquid per minute. A variable frequency driver manufactured by Toshiba is employed to control the total liquid flow rate coarsely, and ball valves are utilized for fine control. Air is supplied via external compressors with a maximum pressure of 0.985 MPa. The operating pressure in the gas line is controlled by a pressure regulator manufactured by Bosch-Pneumatic at 0.689 MPa, and the flow rate is controlled by valves. Both test sections share the common air and water delivery systems. After passing through the test section, the air and water mixture is separated in the water accumulator where the water is recirculated and the air is discharged into the atmosphere.

3.2. Instrumentation

The liquid flow rate is measured by a commercial electromagnetic flowmeter (Honeywell, MagneW3000) and rotameters (Dwyer Instruments, VF series). An electromagnetic flowmeter is employed to measure the total liquid flow rate and rotameters are employed to measure the flow rate of the secondary liquid injection line. The accuracy of the electromagnetic flowmeter and the rotameter is within $\pm 1\%$ of full scale and $\pm 3\%$ of full scale, respectively. The pressure of the gas line is controlled by a pressure regulator (Bosch-Pneumatic) and is kept constant at 100 psi. The gas flow rate is measured by gas rotameters (Dwyer Instruments, RM series). The accuracy of the gas rotameter is within $\pm 4\%$ of full scale. The local pressure is measured by pressure gauges (McDaniel Controls) and the pressure drop along the test section is acquired by a pressure transducer (Honeywell, S900). The accuracy of the pressure gauge and the pressure transducer is within $\pm 3\%$ of span and within $\pm 1\%$ of full scale, respectively.

An impedance-void meter [10] is utilized to obtain an area-averaged impedance signal, which is applied to the analysis of the flow regime identification. Three probe ports are located in each test section at $L/D = 13$, 68 and 133 for the 2.54 cm ID loop and $L/D = 7$, 34, and 67 for the 5.08 cm ID loop. The measurement was made at the central probe port in each loop.

This impedance signal can be converted into the area-averaged void fraction with an impedance-void fraction correlation.

The data acquisition hardware consists of a signal connection electrical circuit block, DC power supply, function generator, acquisition board, and PC. The acquisition board (National Instruments, AT-MIO-64E-3) has a sampling rate of 500 kHz with 12-bit resolution and 64 single-ended or 32 differential-ended channels. The signals are sent to the board via the shielded connector block (National Instruments, SCB-100). The computer is a Dell Dimension XPS-T450 with Pentium III 450 MHz processor. The signal analysis software (National Instruments, LabVIEW) allows constant monitoring of the raw signal during data acquisition.

4. Results and discussion

Series of experimental works were performed for both the vertically upward and vertically downward co-current

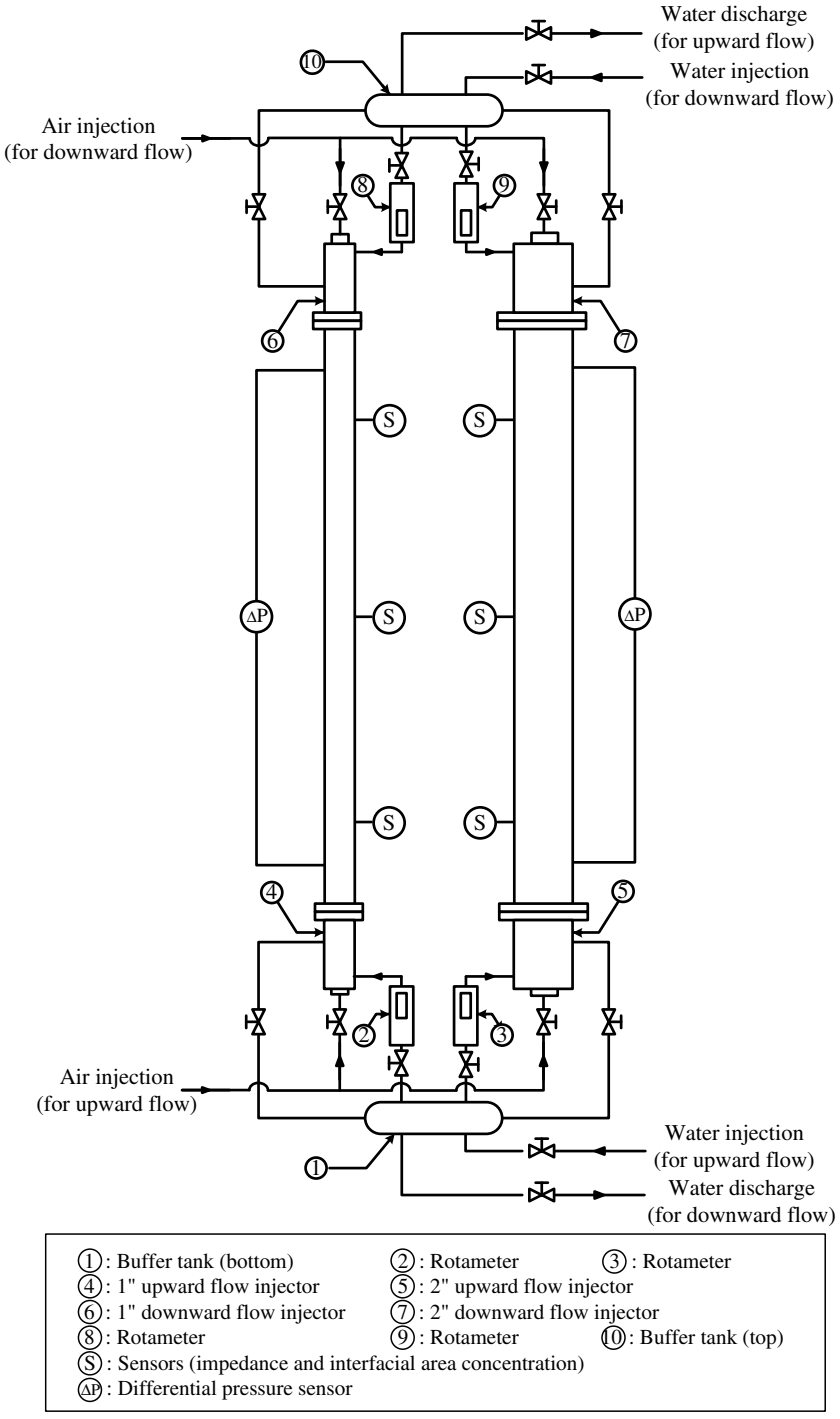

Fig. 14. Schematic diagram of 25.4 mm ID and 50.8 mm ID round vertical air–water upward/downward flow experimental facility (not scaled).

two-phase flow to establish the instantaneous and objective flow regime identification method. Both supervised neural network and self-organized neural network were evaluated to find the optimum structure and better performance in both convergence and prediction.

4.1. Upward two-phase flow

The flow regime map for the upward co-current two-phase flow has been intensively investigated to study the current method with the data relevantly. Furthermore, since there are many reliable transition criteria, the comparison with them is also one of interests in the study.

4.1.1. Characteristics of the impedance signals for the void fraction

Many flow regimes have been suggested based on the geometrical differences: the bubbly flow, slug flow, churn turbulent flow, and annular flow. Sometimes more precise definitions have been also proposed. For the bubbly flow,

the discrete bubbly flow and cap bubbly flow were also distinguished based on the existence of cap bubbles. For the slug flow, the stable slug flow and unstable slug flow were also presented in the literature. As the gas flow rate increases, the size of cap bubble is enlarged and turned into the large Taylor bubble which is named as the slug flow. Tremendously small bubbles occur at the rear part of the Taylor bubble and they are entrapped into the wake region. Although there are still some arguments in the definition of the churn turbulent flow, the impedance signals for churn turbulent flow exhibit very chaotic oscillation. The increase of gas flow finally makes the flow in the annular flow pattern in which the liquid climb over the wall with gas core flow. Various complicated surface waves occurs and runs over the liquid film and liquid droplet due to the break up of the roll wave or solitary wave entrains in to the gas core flow. Therefore, the impedance signals in the annular flow are highly chaotic and low impedance due to the high void fraction.

4.1.2. Supervised neural network

According to the study of Lee et al. [11], the optimized feed forward neural network has the structure of 100 input nodes, 7 hidden nodes, and 5 output nodes. For the input nodes the sorted signals according to the magnitude of 1 s sampling time are used.

The flow regime map for vertically upward flow in 25.4 mm ID pipe determined by the present optimized feed forward neural network was depicted in Fig. 15. The supervised neural networks clearly identified the bubbly flow, cap bubbly flow, slug flow, churn flow. However, the annular flow was difficult to identify due to the lack of data to training. Referring to the study of Mi et al., the present results clearly show that the Mishima–Ishii criteria [13] contained both discrete bubbly flow regime and cap bubbly flow regime. Taitel et al. [4], also classify the discrete bubbly flow and the spherical cap bubbly flow as bubbly flow. Furthermore, the present method actually activates the output nodes with a certain level of confidence, so, there is undetermined identification in the figures which represents that the current neural network activates two competitive regimes with the almost same level of confidence. This indetermination of the flow regime is so natural as pointed by Mishima–Ishii, the flow regime transition is gradual that there should be the mixed flow regimes near the criteria. It was found that the present supervised neural network is capable of identifying the mixed regime on the border of transition. Also, it may be requested to set up the transition criterion for the discrete bubbly to cap bubbly flow regimes. For the transition between the slug flow regime and churn turbulent flow regime, the present identification is in a good agreement with the Mishima–Ishii based on the fully agitated slug bubble in the low liquid flow regime. However, in the higher liquid flow condition, the transition departs from the Mishima–Ishii criteria. Recent arguments on the transition mechanism for the slug-to-churn flow may be caused from this deviation.

Generally speaking, the current flow regime identification with 1 s observation produces the flow regime map successfully in a good agreement with the criteria of Mishima–Ishii.

In the 50.8 mm ID pipe flow, the bubbly-to-slug transition line of Mishima–Ishii penetrates the middle part of the cap bubbly flow as shown in Fig. 16. This means that, in the large pipe diameter, it needs more gas flow to produce large stable Taylor bubble. In this point of view, the cap bubbly regime can be considered as the transition border between the bubbly flow regime and slug flow regime. The criterion based on the geometrical maximum packing of bubbles criteria of Mishima–Ishii can be interpreted as a useful one. But, the criteria need to be modified in the response of the ration of pipe diameter to the length slug bubble. It is partially based on the phenomenological observation that the local distribution of the bubbles

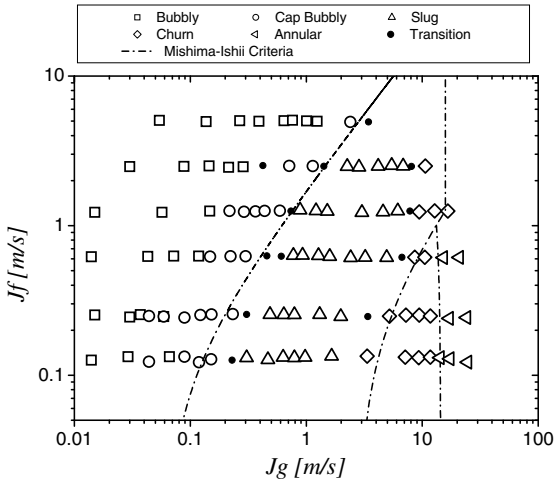

Fig. 15. The flow regime identification results of the present instantaneous supervised neural network for the upward two-phase flow in 25.4 mm ID pipe.

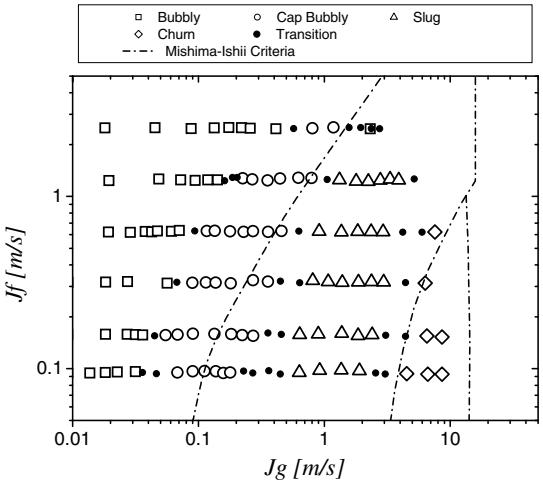

Fig. 16. The flow regime identification results of the present instantaneous supervised neural network for the upward two-phase flow in 50.8 mm ID pipe.

depends on the lift forces acting on the bubbles. The wall peak of the void fraction will enhance the agglomeration of the tiny bubbles, but the lift force for the sufficiently large bubble pushes them to the center of the pipe. Once the local void fraction of the center of pipe exceeds the maximum bubble packing condition, they agglomerate and produce cap bubbles. The local distribution of the bubble and interfacial phenomena are highly complicated as described in the model of the transport equation of the interfacial area concentration of Ishii. Therefore, the present difference between the present result and the Mishima–Ishii may be one of strong motivation to develop the mechanistic model of the evolution of the interfacial area concentration.

For the slug-to-churn transition, the present identification is very close to the criterion of Mishima–Ishii. In the probability density function (PDEF), the churn flow can be classified as the one peak near the Taylor bubble, which means the fully agitated Taylor bubble and its breaking-up produce one large peak of PDEF with wide spectrum near the void fraction of 0.7. Mishima–Ishii has proven that at that point, the mean void fraction is almost equal to the average void fraction of Taylor bubble. Although there are still open arguments on the definition of Churn flow, if we consider the geometrical classification for flow regime, the present method supports the understanding of Mishima–Ishii on churn flow.

4.1.3. Unsupervised neural network

The self-organized neural network, which is not supervised by the designer, classifies the patterns according to the number of clusters. The number of output nodes, therefore, at least exceeds the number of flow patterns which are classified. However, sometimes the unsupervised neural network uses the output nodes to classify the detailed difference in a specific flow pattern not to classify the large group of flow patterns. The optimization of the unsupervised neural network, therefore, means to find the optimum number of output nodes to distinguish the proper flow patterns of interest. In the present study, we change the number of output nodes form three to five to find the proper structure.

As shown in Fig. 17a, three clusters, the bubbly-to-slug transition is well identified by the three clusters KSOM. However, wide range of slug flow was identified as the churn flow. Since KSOM measures the topological Euclidean distance from the center of the cluster, which is selected in the self-training as the most representative data of a certain cluster, the fact that the wide range of slug flow was identified as the churn by KSOM neural network means that in the slug flow, the cluster of unstable slug flow is topologically closer to the cluster of churn flow than that of the slug flow.

However, the four-cluster-KSOM makes some difference as shown in Fig. 17b, four clusters. It is interesting that this increase of cluster number just divides the bubbly flow regime into two: discrete bubble and cap bubble. It

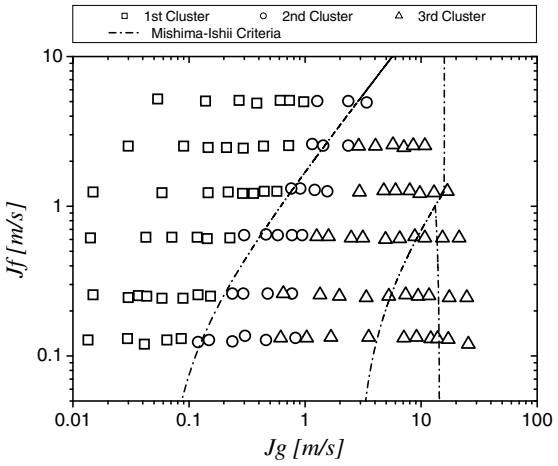

Fig. 17a. The flow regime identification results of Kohonen's self-organized neural network with three clusters for upward flow in 25.4 mm ID pipe.

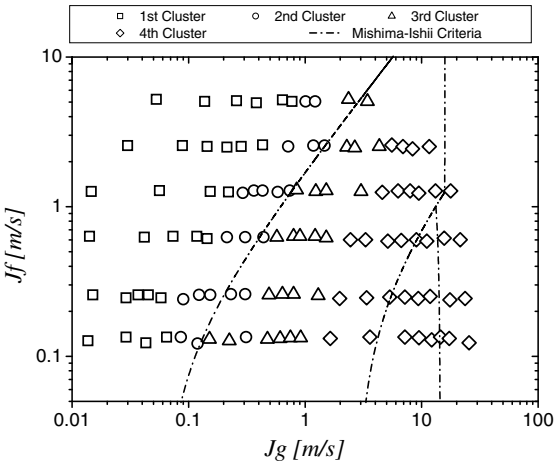

Fig. 17b. The flow regime identification results of Kohonen's self-organized neural network with four clusters for upward flow in 25.4 mm ID pipe.

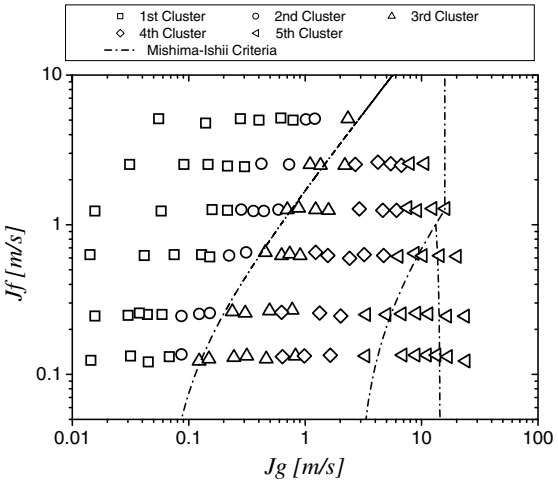

Fig. 17c. The flow regime identification results of Kohonen's self-organized neural network with five clusters for upward flow in 25.4 mm ID pipe.

can be identified by comparing with the result of the supervised flow regime identifier as well as the character of raw signals. However, still large area of the slug flow regime is occupied by the churn flow regime. Therefore, four clusters are identified sensitively in bubbly flow regime but it is insensitive in churn flow regime. The five clusters, Fig. 17c: five clusters, finally, produce almost same level of identification as the supervised method. The bubbly flow regime of Mishima–Ishii is classified in two regimes: dispersed bubbly flow regime and cap bubbly flow regime. Also, the slug flow regime is divided into two: stable slug flow regime and unstable slug flow regime as noted by Whale et al. In consequences, the slug-to-churn transition is very close to Mishima–Ishii criteria.

In the case of upward flow in 50.8 mm ID pipe, the identification results are almost similar to the results of 25.4 mm ID case. As shown in Fig. 18a, three clusters, the bubbly-to-slug transition is also well matched with the three clusters KSOM, and in the case of the four-cluster-KSOM, Fig. 18b: four clusters, the bubbly flow regime is divided into two regimes which are discrete bubble and cap bubble. In the five clusters, Fig. 18c: five clusters, the bubbly flow regime of Mishima–Ishii is classified as two regimes: dispersed bubbly flow regime and cap bubbly flow regime. And the slug flow regime is divided into two: stable slug flow regime and unstable slug flow regime as noted by Whale et al.

The sensitivity of number of cluster to the flow identification is summarized in Tables 1 and 2, respectively. In this point of view, the careless use of output nodes could lead the unrealistic flow regime identification. Because, the topological Euclidean distances among flow regimes measured by the Kohonen self-organized neural network are not proportional to the physical geometrical measure of the flow regimes. Therefore, to identify the churn flow and annular flow, we need to prepare more than five clusters.

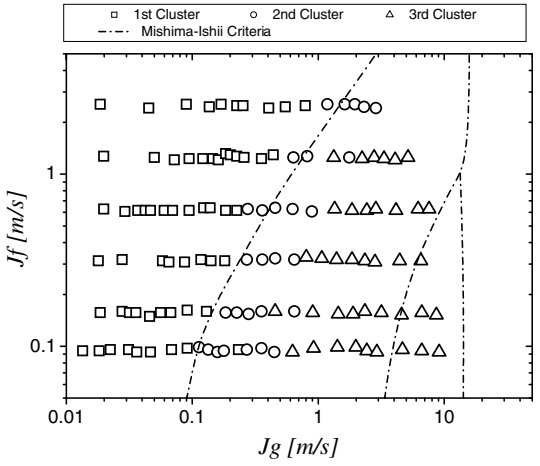

Fig. 18a. The flow regime identification results of Kohonen's self-organized neural network with three clusters for upward flow in 50.8 mm ID pipe.

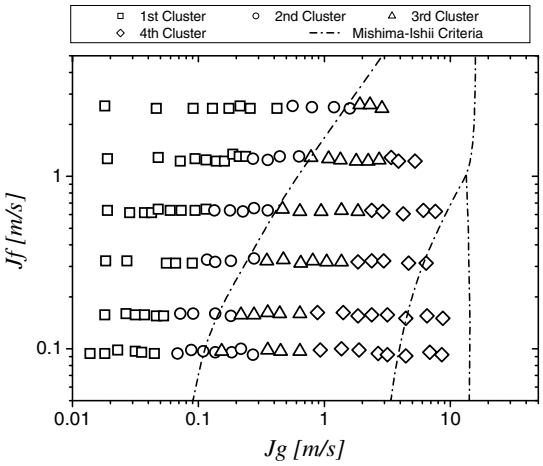

Fig. 18b. The flow regime identification results of Kohonen's self-organized neural network with four clusters for upward flow in 50.8 mm ID.

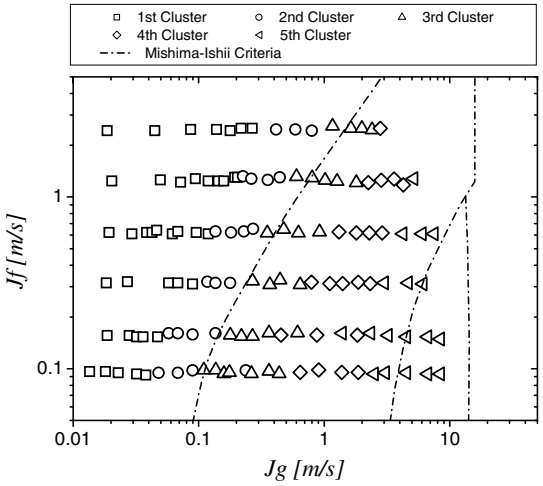

Fig. 18c. The flow regime identification results of Kohonen's self-organized neural network with five clusters for upward flow in 50.8 mm ID.

4.2. Downward two-phase flow

The studies on the downward co-current two-phase flow have not been made intensively when we compare them to the studies on the co-current upward two-phase flow. Furthermore, results are highly influenced by the mixing method of gas and liquid, thus some data and transition criteria of flow regimes are scattered widely among researchers. However, in many cases in the industrial facilities, the co-current downward two-phase flow occurs so that the flow regimes are studied in the present study using the proposed method.

4.2.1. Characteristics of the impedance signals for the void fraction

The visualization using the high speed motion analyzer with 500 frames/s was employed to characterize the flow

Table 1
The sensitivity of number of cluster to the flow regime identification for the upward flow in the pipe of 25.4 mm ID

	Three clusters	Four clusters	Five clusters
First	Bubbly flow	Bubbly flow	Bubbly flow
Second	Stable slug flow	Cap bubbly flow	Cap bubbly flow
Third	Unstable/churn/annular flow	Stable slug flow	Stable slug flow
Fourth		Unstable/churn/annular flow	Unstable slug flow
Fifth			Churn/annular flow

Table 2
The sensitivity of number of cluster to the flow regime identification for the upward flow in the pipe of 50.8 mm ID

	Three clusters	Four clusters	Five clusters
First	Bubbly flow	Bubbly flow	Bubbly flow
Second	Stable slug flow	Cap bubbly flow	Cap bubbly flow
Third	Unstable/churn flow	Stable slug flow	Stable slug flow
Fourth		Unstable/churn flow	Unstable slug flow
Fifth			Churn flow

regimes as shown in Fig. 19. Bubbly flow is basically the same as the upward flow wherein small bubbles are dispersed in a continuous liquid phase. The major difference from the upward flow is that the bubbles tend to migrate towards the center of the tube due to the lift force in the shear flow. However, once cap bubble occurs, the cap bubble attached on the tube wall and makes some spiral motion. Slug flow observed in downward flow is relatively different from upward slug flow. In upward flow, the gas slug, also known as the Taylor bubble, frequently has a bullet shape and its nose faces towards the flow direction. Contrarily, the gas slug in downward flow almost never has a bullet shape; instead, it is more likely a wedge shape and its off-centered nose faces opposite to the flow direction. Churn turbulent flow has the same degree of complex as the upward two-phase flow. Annular flow has the wavy falling film and annular drop flow. For the high gas flow condition, the downward test facility showed the annular drop flow which is very similar to the upward annular flow. Goda et al. [14] made a comparative study of the flow regime map constructed by the method of Mi et al. with the existing flow regime criteria such as Barnea et al. [15] and Usui [16]. The flow regime identification and development of proper constitutive relations for the downward flow may need further works due to the different action of gravity force, which make thicker film in the annular and churn flow regime than the upward case and different bubble migration direction in the bubbly flow. Also, dominant surface waves in the annular flow and entrainment behavior need to be considered in the analysis.

4.2.2. Supervised neural network

Fig. 20 shows the flow regime map for vertically downward flow in 25.4 mm ID pipe determined by the present

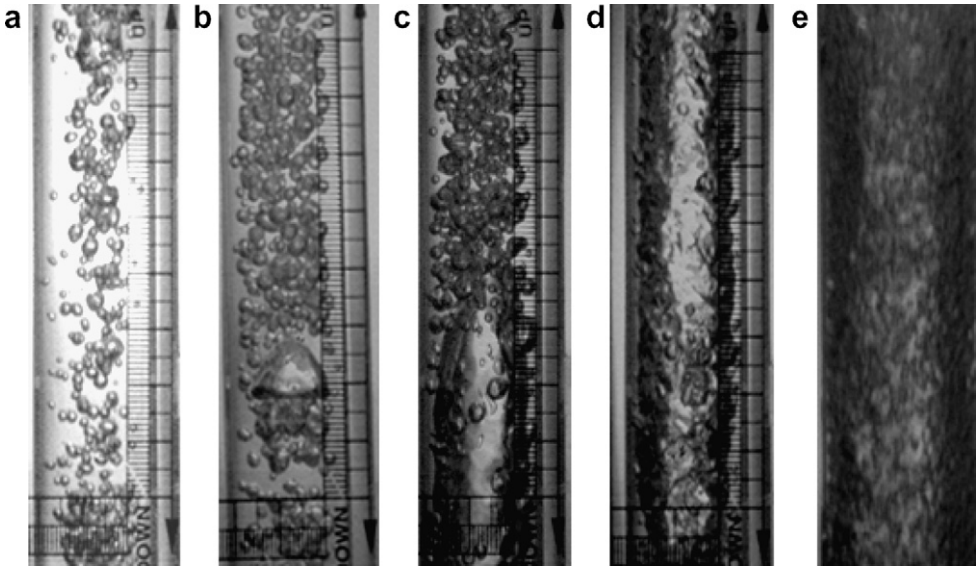

Fig. 19. The representative flow pattern in the vertical co-current downward two-phase flow in a pipe of 2.54 cm ID. (a) Bubbly flow, (b) cap bubbly flow (the nose of cap bubble direct to the wall), (c) the slug flow, (d) churn flow, and (e) the annular flow.

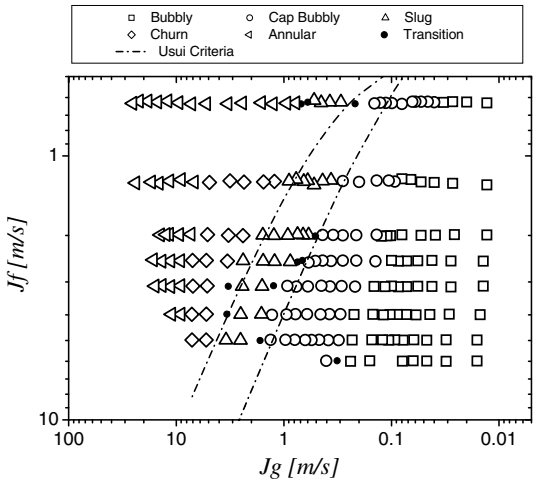

Fig. 20. The flow regime identification results of the present instantaneous supervised neural network for the downward two-phase flow in 25.4 mm ID pipe.

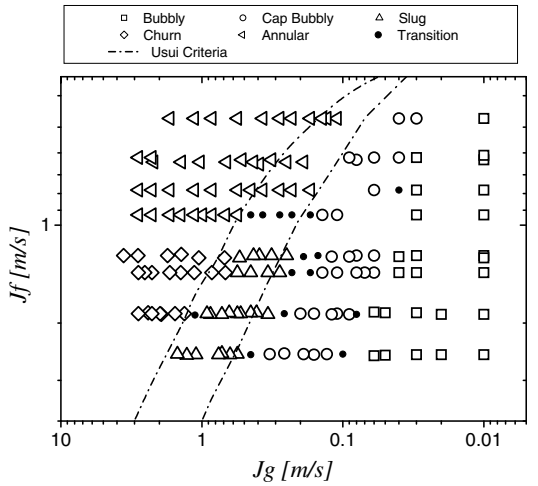

Fig. 21. The flow regime identification results of the present instantaneous supervised neural network for the downward two-phase flow in 50.8 mm ID pipe.

optimized feed forward neural network. It was turned out that the present classification is far away from the criteria of Barnea et al. due to the different injection method of two-phase flow from the current facility as Goda et al. [14] noted. Therefore, in the present study, we only compare the present result with the Usui criteria [16]. Basically the supervised neural network depends seriously on the reference data, so that the present results were fairly representing the flow regimes of Goda et al. which was constructed with the three parameters of PDEF. For the low liquid flow rate region, the sudden transition to the annular flow from the bubbly flow, slug flow, churn flow as increase the gas flow rate was observed. The transition was made due to the kinematic wave which starts form the top injection part. The kinematic wave was not transported for a while but suddenly transported down to the whole pipe and the annular flow pattern occupies the whole pipe. The dynamics of the kinematic wave is very sensitive to the operation procedure such as the increasing operation of decreasing operation of the gas flow and produce a certain types of hysteresis. Goda et al. [14] reported that the unstable region in their flow regime map because in the pipe two different flow regimes coexist for a while due to the stack of the kinematic wave front.

The present result shows clearly, the dispersed bubbly flow, cap bubbly flow, slug flow, churn flow and annular flow regimes. For the 25.4 mm ID tube, the present data are very close to the criteria of Usui [16]. The bubbly-to-slug transition of Usui is well matched the transition from cap bubbly to slug flow regime. The prediction of the slug-to-churn transition of the present method is in a good agreement with the slug-to-annular transition criterion of Usui in which no discrete classification between the churn and annular flow.

Also in the 50.8 mm ID pipe downward flow, the bubbly-to-slug transition line of Usui is close to the results of the present work (Fig. 21), and the slug-to-annular transition follows Usui line except in the region of the low liquid flow rate. This means that in the large pipe diameter, it is difficult to produce large stable Taylor bubble and it is very sensitive to increment of gas flow rate at low liquid velocity. In the low liquid velocity region, the annular like transparent film flow were observed but the impedance signals showed thicker film thickness and large amplitude of the solitary wave. In the present classification we took the reference training data in the low liquid velocity region for the annular flow, so the neural network classify the annular and churn flow. However, as shown in 25.4 mm ID pipe case in which the transition was almost vertical in the plane, i.e. at the constant gas velocity and also in the upward flow case, the transition was at the constant gas velocity, the downward flow also may have the similar transition criterion. In that point of view, the present experiment in the 50.8 mm ID pipe was made in the lower gas velocity condition to clear distinguish the annular and churn transition. It should be noted that this is the matter of definition. The most important factor in the flow pattern classification is the change of dominant phenomena in the interfacial transfer terms. If the interfacial transfer in the annular and churn flow regimes can be estimated by the unified correlation, then there is no reason to make efforts to distinguish these two flow regimes.

The present results made a good agreement with the Usui's criteria for the bubbly-to-slug and slug-to-annular (or churn). It is very hard to distinguish the difference between the annular flow regime and churn flow regime in the 50.8 mm ID pipe.

4.2.3. Unsupervised neural network

Since the supervised neural network has the subjectivity of the researcher due to the selection of reference data for training the neural network, to study the flow regimes identified by the unsupervised neural network is worth to do in

both optimization of the network and the evaluation of the flow regime criteria.

As shown in Fig. 22a, both the bubbly-to-slug transition and the slug-to-annular transition are well identified by the three clusters KSOM. And the four-cluster-KSOM makes some differences as shown in Fig. 22b. The second clusters and the third clusters penetrate the bubbly-to-slug and slug-to-annular transition, respectively. By comparing with the results of the supervised neural network, it is identified as cap bubbly/stable slug regime and unstable slug/ churn regime. The five clusters, Fig. 22c, finally, produce almost same level of identification as the supervised method. The bubbly flow regime of Usui is classified as two regimes which are dispersed bubbly flow and cap bubbly flow regime. Also, the churn flow and annular flow regime are well identified.

In the 50.8 mm ID pipe downward flow, the present method identifies the flow regimes successfully. However, as the number of the clusters increase, the detailed classification was made in the bubbly flow regime and slug flow regime. In the bubbly flow regime, the neural network classifies the discrete bubbly flow and cap bubbly flow. Also in the slug flow, the stable slug and unstable slug were identified. As shown in Fig. 23a, in the three clusters KSOM, both the bubbly-to-slug and slug-to-churn and annular transition are in a good agreement with Usui's criterion. In this case, the distinguishing between the churn and annular flow is not easy because the average film thickness is thicker than the vertical annular case. Furthermore, the existence of solitary wave in the down ward flow which has the large amplitude and propagation speed than small ripples in the upward flow makes difficulty in the classification of the annular flow and churn flow. As increasing the number of clustering node, Fig. 23b, the bubbly flow regime divided into discrete bubble and cap bubble regime.

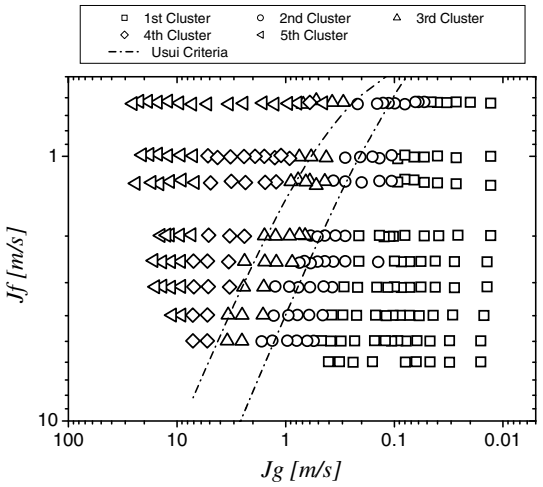

Fig. 22c. The flow regime identification results of Kohonen's self-organized neural network with five clusters for downward flow in 25.4 mm ID.

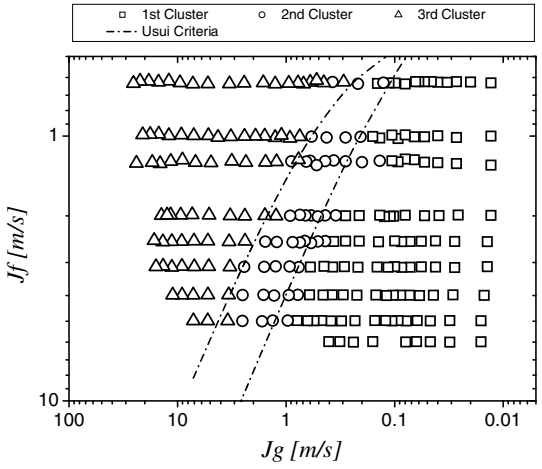

Fig. 22a. The flow regime identification results of Kohonen's self-organized neural network with three clusters for downward flow in 25.4 mm ID pipe.

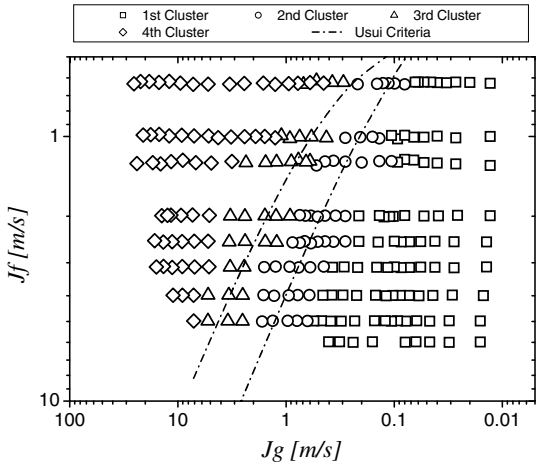

Fig. 22b. The flow regime identification results of Kohonen's self-organized neural network with four clusters for downward flow in 25.4 mm ID.

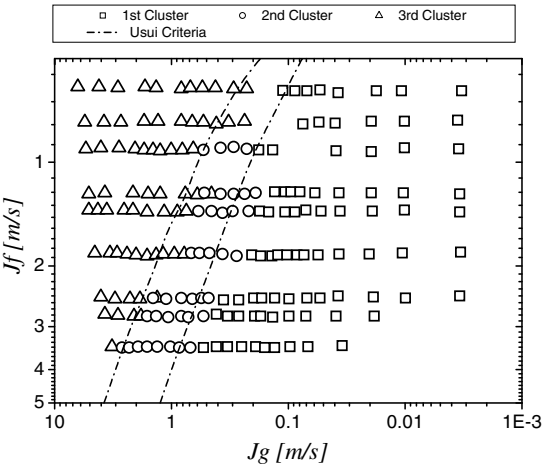

Fig. 23a. The flow regime identification results of Kohonen's self-organized neural network with three clusters for downward flow in 50.8 mm ID.

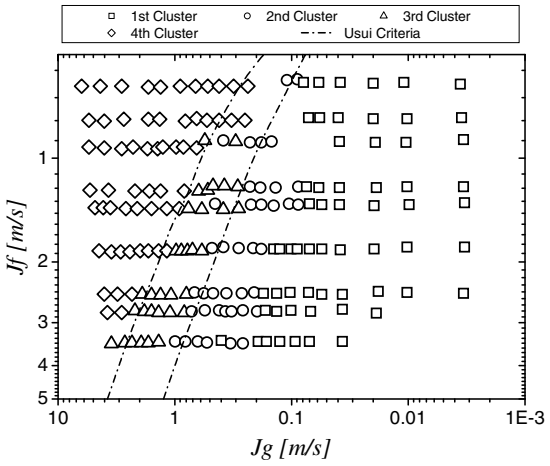

Fig. 23b. The flow regime identification results of Kohonen's self-organized neural network with four clusters for downward flow in 50.8 mm ID pipe.

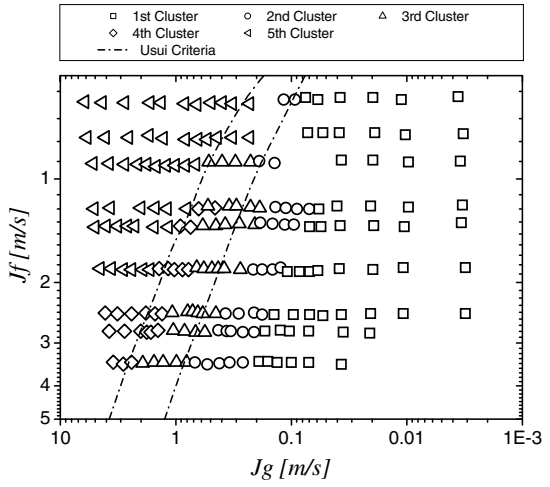

Fig. 23c. The flow regime identification results of Kohonen's self-organized neural network with five clusters for downward flow in 50.8 mm ID pipe.

The five clusters KSOM makes little differences to the result of supervised method as presented in Fig. 23c. In this case, the incensement of output node is affected to the division between stable slug flow and unstable slug flow regime. It means that the transition between stable slug and unstable slug is more dominant to the slug-to-churn transition from a view of the topological Euclidean distance. The sensitivity of number of cluster to the flow identification is summarized in Tables 3 and 4, respectively.

5. Conclusions

A method of objective and instantaneous flow regime identification was developed here to meet the needs in the practical two-phase flow such as the rapid transition or unstable state under the incident or weak gravity field. On the behalf of the objective nature of the neural network and their relaxed restriction in data handling, the present method was actualized by the probability distribution functional input of short sampling period, considerably instantaneous to the neural network.

The complexity in the network structure due to the increased number of input nodes to accept the sorted data was accommodated through sensitivity study for the optimization of the network. The experimental data for both co-current upward and downward two-phase flow from the two-phase flow loop of 25.4 mm ID and 50.8 mm ID at Purdue University were used to develop the flow regime map using the present instantaneous and objective method. It was found that the present method could identify flow regime within the short period observation of 1 s, successfully, for both upward and downward flow. For the upward two-phase flow, both supervised and unsupervised methods agree with the transition criteria of Mishima and Ishii. However, for the downward flow, the existing criteria need to be modified due to the pipe diameter effect on the flow regime.

Table 3
The sensitivity of number of cluster to the flow regime identification for the downward flow in the pipe of 25.4 mm ID

	Three clusters	Four clusters	Five clusters
First	Bubbly flow	Bubbly flow	Bubbly flow
Second	Slug flow	Cap bubbly/stable slug flow	Cap bubbly flow
Third	Churn/annular flow	Unstable slug/churn flow	Slug flow
Fourth		Churn/annular flow	Churn flow
Fifth			Annular flow

Table 4
The sensitivity of number of cluster to the flow regime identification for the downward flow in the pipe of 50.8 mm ID

	Three clusters	Four clusters	Five clusters
First	Bubbly flow	Bubbly flow	Bubbly flow
Second	Slug flow	Cap bubbly flow	Cap bubbly flow
Third	Churn/annular flow	Slug flow	Stable slug flow
Fourth		Churn/annular flow	Unstable slug flow
Fifth			Churn/annular flow

Acknowledgement

The work was supported partially by the school of Nuclear Engineering of Purdue University for Dr. J.Y. Lee during his staying in the school as a visiting professor and supported in part by the Ministry of Science and Technology (MOST) of Korean Government in the program of the Basic Atomic Energy Research Institute (BAERI). Also, the effort to prepare a part of data by Mr. Paranjape is greatly acknowledged.

References

[1] M. Ishii, Thermo-Fluid Dynamic Theory of Two-Phase Flow, Eyrolles, Paris, 1975.
[2] M. Ishii, Objective characterization of interfacial structure in two-phase flow, Keynote Speak, NURETH-10, Seoul, 2003, KL-01.
[3] P. Griffith, G.B. Wallis, Two-phase slug flow, J. Heat Transfer 83 (1961) 307–320.
[4] Y. Taitel, D. Barnea, A.E. Dukler, Modeling flow pattern transitions for steady upward gas–liquid flow in vertical tubes, AIChE J. 26 (1980) 345–354.
[5] R.C. Fernandes, R. Semiat, A.E. Duckler, Hydrodynamic model for gas–liquid slug flow in vertical tubes, AIChE J. 32 (1983) 981–989.
[6] A.R. Hassan, C.S. Kabir, Two-phase flow in vertical and inclined annuli, Int. J. Multiphase Flow 18 (1992) 279–293.
[7] M.A. Vince, R.T. Lahey, On the development of an objective flow regime indicator, Int. J. Multiphase Flow 8 (1982) 93–124.
[8] O.C. Jones, N. Zuber, The interrelation between void fraction fluctuations and flow patterns in two-phase flow, Int. J. Multiphase Flow 2 (1975) 273–534.
[9] Y. Mi, M. Ishii, L.H. Tsoukalas, Flow regime identification methodology with neural networks and two-phase flow models, Nuclear Eng. Des. 204 (2001) 87–100.
[10] Y. Mi, M. Ishii, L.H. Tsoukalas, Vertical two-phase flow identification using advanced instrumentation and neural networks, Nucl. Eng. Des. 204 (1998) 409–420.
[11] J.Y. Lee, N.S. Kim, M. Ishii, An instantaneous flow regime identification using probability distribution function and feed forward neural network, in: Proceedings of 10th International Topical Meeting on Nuclear Reactor Thermal Hydraulics (NURETH-10), Seoul, 2003, A00309.
[12] T. Kohonen, Self-Organizing Maps, vol. 30, Springer, New York, 1995.
[13] K. Mishima, M. Ishii, Flow regime transition criteria for upward two-phase flow in vertical tubes, Int. J. Heat Mass Transfer 27 (1984) 723–737.
[14] H. Goda, S. Kim, Y. Mi, J. Finch, M. Ishii, J. Uhle, Flow regime identification of co-current downward two-phase flow with neural network approach, in: Proceedings of 10th International Conference of Nuclear Engineering (11ICONE-10), Arlington, VA, 2002, p. 22088.
[15] D. Barnea, O. Shnam, Y. Taitel, Flow Pattern transition for vertical downward two-phase flow, Chem. Eng. Sci. 37 (1982) 741–744.
[16] K. Usui, Vertically downward two-phase flow: II. Flow regime transition criteria, J. Nucl. Sci. Technol. 26 (1989) 1013–1022.